Functional Characterization of Mammalian Inositol 1,4,5-Trisphosphate Receptor Isoforms

Huiping Tu,* Zhengnan Wang,* Elena Nosyreva,* Humbert De Smedt,† and Ilya Bezprozvanny*
*Department of Physiology, University of Texas Southwestern Medical Center at Dallas, Dallas, Texas 75390 USA; and
†Laboratorium voor Fysiologie, K.U.Leuven, B-3000, Leuven, Belgium

ABSTRACT Inositol 1,4,5-trisphosphate receptors ($InsP_3R$) play a key role in intracellular calcium (Ca^{2+}) signaling. Three mammalian $InsP_3R$ isoforms—$InsP_3R$ type 1 ($InsP_3R1$), $InsP_3R$ type 2 ($InsP_3R2$), and $InsP_3R$ type 3 ($InsP_3R3$) are expressed in mammals, but the functional differences between the three mammalian $InsP_3R$ isoforms are poorly understood. Here we compared single-channel behavior of the recombinant rat $InsP_3R1$, $InsP_3R2$, and $InsP_3R3$ expressed in Sf9 cells, reconstituted into planar lipid bilayers and recorded with 50 mM Ba^{2+} as a current carrier. We found that: 1), for all three mammalian $InsP_3R$ isoforms the size of the unitary current is 1.9 pA and single-channel conductance is 74–80 pS; 2), in optimal recording conditions the maximal single-channel open probability for all three mammalian $InsP_3R$ isoforms is in the range 30–40%; 3), in optimal recording conditions the mean open dwell time for all three mammalian $InsP_3R$ isoforms is 7–8 ms, the mean closed dwell time is ~10 ms; 4), $InsP_3R2$ has the highest apparent affinity for $InsP_3$ (0.10 μM), followed by $InsP_3R1$ (0.27 μM), and then by $InsP_3R3$ (0.40 μM); 5), $InsP_3R1$ has a high-affinity (0.13 mM) ATP modulatory site, $InsP_3R2$ gating is ATP independent, and $InsP_3R3$ has a low-affinity (2 mM) ATP modulatory site; 6), ATP modulates $InsP_3R1$ gating in a noncooperative manner ($n_{Hill} = 1.3$); 7), ATP modulates $InsP_3R3$ gating in a highly cooperative manner ($n_{Hill} = 4.1$). Obtained results provide novel information about functional properties of mammalian $InsP_3R$ isoforms.

INTRODUCTION

The inositol (1,4,5)-trisphosphate receptor ($InsP_3R$) is an intracellular calcium (Ca^{2+}) release channel that plays a key role in Ca^{2+} signaling in cells (Berridge, 1993). Three $InsP_3R$ isoforms—$InsP_3R$ type 1 ($InsP_3R1$), $InsP_3R$ type 2 ($InsP_3R2$), and $InsP_3R$ type 3 ($InsP_3R3$) are expressed in mammals (Furuichi et al., 1994), each with a unique expression pattern. $InsP_3R1$ is predominant in the central nervous system, but most other tissues express at least two and often all three $InsP_3R$ isoforms at different ratios (Taylor et al., 1999). The $InsP_3R$ is a large (~1 MDa) tetrameric complex (Furuichi et al., 1994). The three mammalian $InsP_3R$ isoforms are 60–70% identical in sequence (Furuichi et al., 1994) and share a common domain structure (Mignery and Sudhof, 1990; Miyawaki et al., 1991) that consists of an amino-terminal $InsP_3$-binding domain, a carboxy-terminal Ca^{2+} channel domain, and a middle coupling domain containing most of the putative regulatory sites. The $InsP_3$-binding and Ca^{2+} channel-forming domains are highly conserved between $InsP_3R$ isoforms, whereas the middle coupling domain is the most divergent.

Functional properties of native and recombinant $InsP_3R1$ have been extensively characterized by Ca^{2+} flux measurements, planar lipid bilayer or nuclear envelope patch-clamp recordings (reviewed in Bezprozvanny and Ehrlich, 1995; Thrower et al., 2001). In contrast with $InsP_3R1$, functional properties of $InsP_3R2$ and $InsP_3R3$ are less known (Thrower et al., 2001). The functional properties of purified native cardiac $InsP_3R2$ (Ramos-Franco et al., 1998), purified recombinant $InsP_3R2$ expressed in COS cells (Ramos-Franco et al., 2000), and native $InsP_3R3$ from RINm5F cells (Hagar et al., 1998; Hagar and Ehrlich, 2000) were characterized in planar lipid bilayers. The functional properties of recombinant $InsP_3R3$ expressed in *Xenopus* oocytes were described in nuclear envelope patch-clamp experiments (Mak et al., 2001a,b, 2000). Some of these studies resulted in conflicting data, but because of differences in techniques, experimental conditions and expression systems used by various groups, systematic comparison of obtained results is difficult.

Ca^{2+} signals supported by different endogenous chicken $InsP_3R$ isoforms have been previously compared in a Ca^{2+} imaging study with genetically altered DT40 cells by systematically deleting two out of three isoforms (Miyakawa et al., 1999). In the latter approach, however, comparison of functional properties of the three $InsP_3R$ isoforms is complicated by the differences in the endogenous expression levels of each isoform in DT40 cells. To compare single-channel properties of mammalian $InsP_3R$ isoforms in identical conditions, here we expressed rat $InsP_3R1$, $InsP_3R2$, and $InsP_3R3$ in *Spodoptera frugiperda* (Sf9) cells. The recombinant $InsP_3R$ isoforms were reconstituted into planar lipid bilayers and characterized in identical recording conditions using 50 mM Ba^{2+} as a current carrier. The Ca^{2+} imaging results obtained in DT40 cells (Miyakawa et al., 1999) formed a framework for interpretation of single-channel data with different $InsP_3R$ isoforms obtained in our experiments. Our results provide a first comprehensive

Submitted July 14, 2004, and accepted for publication October 29, 2004.

Address reprint requests to Dr. Ilya Bezprozvanny, Dept. of Physiology, K4.112 UT Southwestern Medical Center at Dallas, 5323 Harry Hines Blvd., Dallas, TX 75390-9040. Tel.: 214-648-6737; Fax: 214-648-2974; E-mail: Ilya.bezprozvanny@utsouthwestern.edu.

0006-3495/05/02/1046/10 $2.00

doi: 10.1529/biophysj.104.049593

description of single-channel properties of the three mammalian $InsP_3R$ isoforms in identical experimental conditions.

MATERIALS AND METHODS

Generation of recombinant baculoviruses

The baculoviruses expressing rat $InsP_3R1$ (RT1) and rat $InsP_3R3$ (RT3) have been previously described (Maes et al., 2000; Tu et al., 2002). To generate rat $InsP_3R2$-encoding baculovirus (RT2) a coding sequence of rat $InsP_3R2$ in pCMV5 vector (Ramos-Franco et al., 2000; Sudhof et al., 1991) was subcloned into pFastBac1 vector (Invitrogen, Carlsbad, CA) and 5′ untranslated region (UTR) was replaced with the Kozak sequence by PCR using the *Bss*HII (5′ UTR) and *Sfi*I (2143) restriction sites. The RT2 baculoviruses were generated and amplified using the Bac-to-Bac system according to the manufacturer's (Invitrogen) instructions.

Expression of $InsP_3R$ in Sf9 cells

S. frugiperda (Sf9) cells were obtained from American Type Culture Collection (Manassas, VA) and cultured in suspension culture in supplemented Grace's insect media (Invitrogen) with 10% fetal bovine serum at 27°C. The three isoforms of $InsP_3R$ (RT1, RT2, and RT3) were expressed in Sf9 cells as previously described for RT1 (Nosyreva et al., 2002; Tu et al., 2002). Briefly, 150 ml of Sf9 cell culture was infected by $InsP_3R$-encoding baculoviruses at multiplicity of infection (MOI) of 5–10. Sf9 cells were collected 66–72 h postinfection by centrifugation at 4°C for 5 min at 800 rpm (GH 3.8 rotor, Beckman Instruments, Fullerton, CA). The cellular pellet was resuspended in 25 ml of homogenization buffer A (0.25 M sucrose, 5 mM Hepes, pH 7.4) supplemented with protease inhibitors cocktail (1 mM EDTA, aprotinin 2 μg/ml, leupeptin 10 μg/ml, benzamidine 1 mM, 4-(2-aminoethyl)-benzenesulfonyl fluoride hydrochloride 2.2 mM, pepstatin 10 μg/ml, phenylmethylsulfonyl fluoride 0.1 mg/ml). Cells were disrupted by sonication (Branson Ultrasonics, Danbury, CT) and manually homogenized on ice with a glass-Teflon homogenizer.

The microsomes were isolated from the Sf9 cell homogenate by differential centrifugation as previously described (Kaznacheyeva et al., 1998). Briefly, 25 ml of Sf9 cell homogenate was centrifuged for 15 min at 4 k g_{max} (J 25.50 rotor, Beckman Instruments). The supernatant fluid was filtered through cheese cloth, and the filtrate was centrifuged for 30 min at 90 k g_{max} (Ti 50.2 rotor, Beckman Instruments). The pellet from the latter spin was resuspended in 25 ml of high-salt buffer B (0.6 M KCl, 5 mM NaN_3, 20 mM $Na_4P_2O_7$, 1 mM EDTA, 10 mM HEPES, pH 7.2) and manually homogenized on ice using Teflon/glass manual homogenizer and centrifuged for 15 min at 4 k g_{max} (J 25.50 rotor, Beckman Instruments). The resulting supernatant fluid was centrifuged for 30 min at 90 k g_{max} (Ti 50.2 rotor, Beckman Instruments). The pellet from the last spin was resuspended in 0.5 ml of the storage buffer (10% sucrose, 10 mM 3-morpholinopropanesulfonic acid, pH 7.0) to typically yield 6 mg/ml of protein (Bradford assay, Bio-Rad), aliquoted, quickly frozen in liquid nitrogen, and stored at −80°C.

Expression of $InsP_3R$ isoforms was confirmed by Western blotting with isoform-specific antibodies. Rabbit polyclonal anti-$InsP_3R1$ antibody T443 was previously described (Kaznacheyeva et al., 1998). Rabbit polyclonal anti-$InsP_3R2$ (IB7122) and anti-$InsP_3R3$ (IB7124) antibodies were generated against keyhole limpet haemocyanin-conjugated $InsP_3R2$ (RLGFLGSNTPHENHHMPPH) and $InsP_3R3$ (RLGFVDVQNCMSR) carboxy-terminal peptides and affinity purified (AP) on antigenic peptides conjugated to *N*-hydroxysuccinimide-activated Sepharose (Amersham-Pharmacia Biotech).

Single-channel recordings of $InsP_3R$ activity

Planar lipid bilayers were formed from dioleoyl-phosphoethanolamine/dioleoyl-phosphoserine (3:1) synthetic lipid (Avanti Polar Lipids, Alabaster, AL) mixture in decane on the small (100–200 μm in diameter) hole in Teflon film separating two chambers 3 ml each (*cis* and *trans*). Before formation of the bilayer the hole was prepainted with phytanoyl-phosphocholine/dioleoyl-phosphoserine (3:1) synthetic lipid (Avanti Polar Lipids) mixture in decane. Recombinant $InsP_3R$ isoforms were incorporated into planar lipid bilayers by microsomal vesicle fusion as described previously for the wild-type and mutant $InsP_3R1$ (Nosyreva et al., 2002; Tu et al., 2002). In these experiments endoplasmic reticulum (ER) microsomes were added to the *cis* chamber with stirring, and fusion of microsomes to the bilayer was induced by osmotic pressure resulting from an addition of 0.6–1 M KCl to the *cis* chamber. Fusion of ER microsomes to the bilayer leads to incorporation of the channels in such an orientation that the *cis* side is equivalent to cytosol and the *trans* side is equivalent to the lumen of ER (Miller, 1986). Fusion of ER vesicles with the bilayer was registered by the appearance of chloride currents. Once sufficient fusion was achieved (>100 pA of chloride currents), *cis* chamber (cytosolic) was perfused with 20 vol of *cis* recording solution (110 mM Tris dissolved in HEPES, pH 7.35) with stirring. The *trans* chamber (luminal) was filled with *trans* recording solution (50 mM $Ba(OH)_2$ dissolved in HEPES, pH 7.35), leaving 50 mM Ba^{2+} as a main charge carrier (Bezprozvanny and Ehrlich, 1994). The *cis* chamber was held at virtual ground and the *trans* chamber was voltage clamped (Warner OC-725C bilayer clamp) in the range of membrane potentials (*cis* chamber potential relative to *trans* chamber potential) from +10 to −30 mV as indicated in the text. The liquid junction potential between *cis* and *trans* recording solutions was compensated before formation of the bilayer.

The $InsP_3R$ single-channel currents were amplified (Warner OC-725C), filtered at 1 kHz by low-pass eight-pole Bessel filter (model 900, Frequency Devices, Haverhill, MA), digitized at 5 kHz (Digidata 1200, Axon Instruments, Union City, CA), stored on a computer hard drive and recordable optical disks, and analyzed offline using pClamp 6 (Axon Instruments) and WinEDR V2.3 (Dempster, 2001). For single-channel analysis currents were filtered digitally at 500 Hz, and for presentation of the current traces data were filtered at 200 Hz. All-points amplitude histograms were generated from current records at least 100-s long and fit by a sum of two Gaussian functions (WinEDR V2.3). Channel openings were detected by half-threshold ($t \geq 2$ ms) crossing criteria (Sakmann and Neher, 1983) using pClamp 6. We have not corrected for missed events in our analysis. Open and closed dwell-time distributions were fit by a single exponential fit (pClamp 6).

$InsP_3$- and ATP-dependence of $InsP_3R$ was determined as described in (Bezprozvanny and Ehrlich, 1993; Lupu et al., 1998) by consecutive additions to the *cis* chamber from the concentrated stocks (1 mM $InsP_3$ or 100 mM and 500 mM Na_2ATP) with at least 30 s stirring of solutions in both chambers. Evidence for the presence of multiple channels in the bilayer (multiple open levels) was obtained in the majority of the experiments. The number of active channels in the bilayer was estimated as a maximal number of simultaneously open channels during the course of an experiment (Horn, 1991). The probability of the closed level, and first and second open levels was determined by using half-threshold crossing criteria ($t \geq 2$ ms) from the records lasting at least 100 s at each $InsP_3$ or ATP concentrations. The single-channel open probability (*Po*) was calculated using the binomial distribution for the levels 0, 1, and 2, and assuming that the channels in the bilayer were identical and independent (Colquhoun and Hawkes, 1983). Potential errors of absolute *Po* values associated with the possible underestimate of the number of active channels in the bilayer were minimized by normalizing the *Po* to the maximum *Po* observed in the same experiment. The normalized data from several experiments with each $InsP_3R$ isoform were averaged together for presentation and fitting. The fits were generated using least-squares routine (SigmaPlot 2001, Jandel Scientific, San Rafael, CA) and the quality of the fit was evaluated from the coefficient of determination (R^2). The standard errors of resulting parameters were obtained as the estimates of the uncertainties in the values of regression coefficients obtained as a result of the fitting procedure (SigmaPlot 2001, Jandel Scientific).

To obtain the parameters of $InsP_3$ dependence, the normalized and averaged data were fit by the equation

$$P[InsP_3] = P_m[InsP_3]^n/(k_{InsP3}^n + [InsP_3]^n), \quad (1)$$

modified from Lupu et al. (1998), where P_m is the maximal normalized open probability, n is the Hill coefficient, and k_{InsP3} is the apparent affinity for $InsP_3$.

To obtain the parameters of ATP dependence, the normalized and averaged data were fit by the equation

$$P[ATP] = P0 + P_m[ATP]^n/(k_{ATP}^n + [ATP]^n), \quad (2)$$

modified from Bezprozvanny and Ehrlich (1993), where $P0$ is the normalized open probability in the absence of ATP, P_m is the maximal increase in normalized Po induced by ATP, n is the Hill coefficient, and k_{ATP} is the apparent affinity for ATP.

RESULTS

Expression and functional properties of mammalian $InsP_3R$ isoforms

The baculoviruses encoding rat $InsP_3R1$ (RT1) and rat $InsP_3R3$ (RT3) have been previously described (Maes et al., 2000; Tu et al., 2002). The baculovirus encoding rat $InsP_3R2$ (RT2) has been generated as described in Materials and Methods. The *S. frugiperda* (Sf9) cells infected with RT1, RT2, and RT3 baculoviruses were used to prepare microsomes 66–72 h postinfection as described in Materials and Methods. The microsomes prepared from noninfected Sf9 cells (Sf9) and from RT1-, RT2-, or RT3-infected Sf9 cells were analyzed by Western blotting with anti-$InsP_3R1$ T443 antibodies (Fig. 1 *A*), anti-$InsP_3R2$ affinity purified IB7122-AP antibodies (Fig. 1 *B*), and anti-$InsP_3R3$ affinity purified IB7124-AP antibodies (Fig. 1 *C*). A prominent immunoreactive band of ~260 kDa was detected in samples from baculovirus-infected cells, but not in noninfected control samples (Fig. 1, *A–C*). The specificity of the isoform-specific $InsP_3R$ antibodies used in these experiments is supported by the lack of cross-reactivity with microsomes from RT1, RT2, and RT3-infected Sf9 cells (Fig. 1, *A–C*). Our results support efficient expression of full-length rat $InsP_3R1$, $InsP_3R2$, and $InsP_3R3$ in RT1-, RT2-, and RT3-infected Sf9 cells in our experimental conditions.

As we previously described (Nosyreva et al., 2002; Tu et al., 2002, 2003), when the microsomes isolated from RT1-infected Sf9 cells were fused with planar lipid bilayers, $InsP_3$-gated channel activity was frequently (60/70) observed (Fig. 2 *A*). In contrast, the $InsP_3$-gated channels were never ($n = 10$) observed in the experiments with microsomes isolated from uninfected Sf9 cells (Nosyreva et al., 2002; Tu et al., 2002, 2003). Similar to experiments with microsomes from RT1-infected Sf9 cells, $InsP_3$-gated channels were frequently observed in experiments with microsomes from RT2-infected Sf9 cells (35/40) (Fig. 3 *A*) and with microsomes from RT3-infected Sf9 cells (40/46) (Fig. 4 *A*). Most of the experiments with microsomes from RT1-, RT2-, and RT3-infected Sf9 cells resulted in incorporation of multiple active $InsP_3R$ in the bilayer. To compare the basic channel properties of recombinant $InsP_3R1$, $InsP_3R2$, and $InsP_3R3$ we performed single-channel analysis of currents recorded in a few experiments with only a single active $InsP_3R$ in the bilayer for each

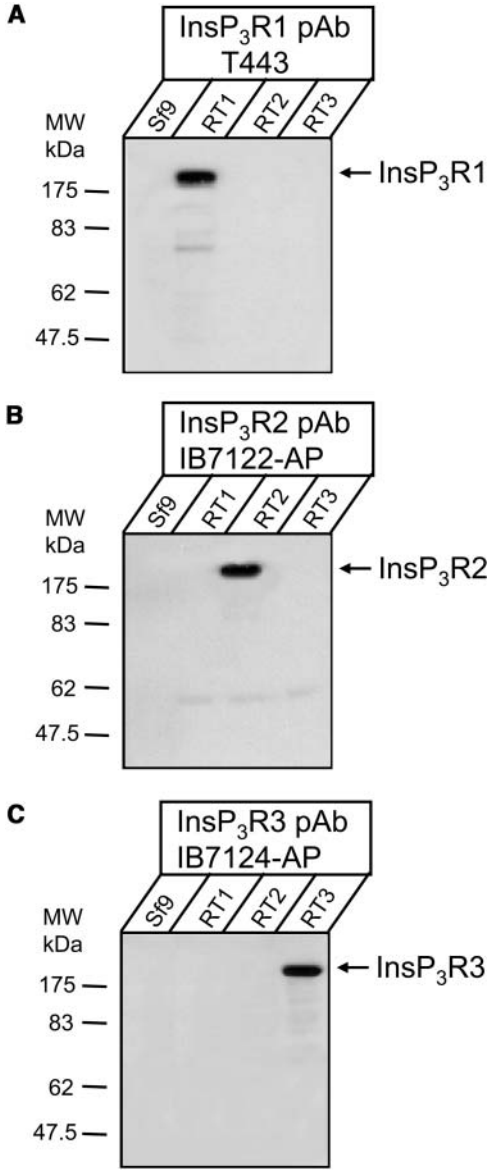

FIGURE 1 Expression of mammalian $InsP_3R$ isoforms in Sf9 cells. Western blot of microsomal proteins. Microsomes isolated from noninfected Sf9 cells (*Sf9*) and from Sf9 cells infected with RT1, RT2, and RT3 baculoviruses were analyzed by Western blotting with polyclonal antibodies specific for $InsP_3R1$ (*A*), $InsP_3R2$ (*B*), and $InsP_3R3$ (*C*) as indicated. For each microsomal preparation, 10 μg of total protein was loaded on the gel.

$InsP_3R$ isoform (as judged by the absence of multiple open levels). From this analysis we determined that in standard recording conditions (pCa 6.7, 0.5 mM ATP, 2 μM $InsP_3$), $InsP_3R1$ and $InsP_3R2$ displayed similar levels of activity with Po values of ~30% (Figs. 2 *A* and 3 *A*; Table 1). In contrast, $InsP_3R3$ channels were less active in standard recording conditions, with Po values <5% (Fig. 4 *A*; Table 1).

All-points current amplitude histograms for each $InsP_3R$ isoform were fit by a sum of two Gaussian functions corresponding to the closed and open states of the channels

(panel *B* in Figs. 2–4). Thus, all three $InsP_3R$ isoforms open primarily to the main conductance state and subconductance states (Watras et al., 1991) are infrequent. At 0 mV holding potential, the size of the unitary current for the main conductance state of all 3 $InsP_3R$ isoforms in our experimental conditions was close to 1.9 pA (Figs. 2 *B*, 3 *B*, and 4 *B*; Table 1). The open dwell time distribution was fit by a single exponential function (Figs. 2 *C* and 3 *C*) with the mean open time in the range 7–8 ms for $InsP_3R1$ and $InsP_3R2$ isoforms (Table 1). The dwell closed time distribution was also fit by a single exponential function (Figs. 2 *D* and 3 *D*) with the mean closed time close to 10 ms for $InsP_3R1$ and $InsP_3R2$ (Table 1). Because of the low frequency of openings (Fig. 4), we were not able to collect enough events to perform kinetic analysis of $InsP_3R3$ channels in standard recording conditions. To further characterize the conductance properties of three mammalian $InsP_3R$ isoforms, we measured the unitary currents supported by these channels at various transmembrane potentials between +10 and −30 mV (Fig. 5). The slope of the resulting current-voltage relationship provided us with the values of single-channel conductance equal to 80.0 ± 0.3 pS ($n = 6$) for RT1, 78.0 ± 0.5 pS ($n = 4$) for RT2, and 74 ± 0.4 pS ($n = 3$) for RT3 (Fig. 5; Table 1).

$InsP_3$ sensitivity of mammalian $InsP_3R$ isoforms

In the next series of experiments we studied the sensitivity of mammalian $InsP_3R$ isoforms to $InsP_3$. The channel activity was recorded at pCa 6.7 in the presence of 0.5 mM ATP and in the range from 50 nM to 2 μM of $InsP_3$ concentrations for $InsP_3R1$ and $InsP_3R2$ and in the range from 50 nM to 10 μM range of $InsP_3$ concentrations for $InsP_3R3$. Because most of the experiments resulted in multichannel bilayers, the *Po* values in each experiment were normalized to the maximal *Po*

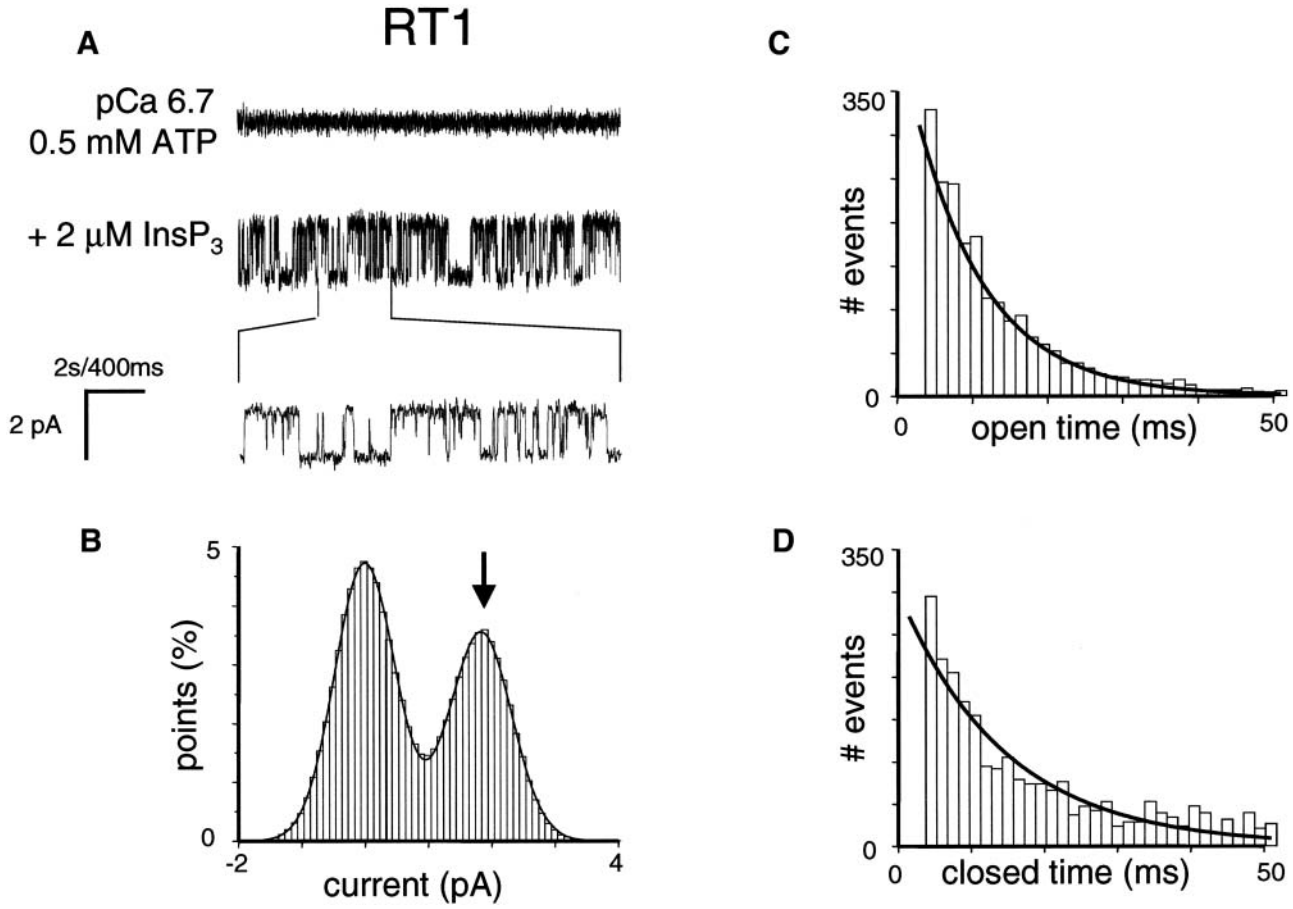

FIGURE 2 Single-channel properties of recombinant rat $InsP_3R1$ (*RT1*). (*A*) Single-channel records of recombinant $InsP_3R1$ in planar lipid bilayers. The experiments were performed at pCa 6.7 in the presence of 0.5 mM ATP (*top trace*). Addition of 2 μM $InsP_3$ to the *cis* (cytoplasmic) side activated $InsP_3R1$ (*middle trace*). Current trace at the expanded timescale is also shown (*bottom trace*). (*B–D*) Analysis of the $InsP_3R1$ single-channel currents. All-points current amplitude histogram (*B*), open dwell time distribution (*C*), and closed dwell time distribution (*D*) are shown. The amplitude histogram (*B*) was fitted with a sum of two Gaussian functions corresponding to closed and open states of the $InsP_3R1$. The Gaussian peak corresponding to an open state of $InsP_3R1$ (*arrow*) was centered at 1.82 pA, had $\sigma = 0.49$ pA, and area 41%. Open and closed time distributions (*C* and *D*; number of events = 5000) were fitted with a single exponential function (*curves*) that yielded mean open time $\tau_0 = 6.9$ ms and mean closed time $\tau_c = 10.1$ ms. The data from the same experiment were used for panels *A–D*. Similar analysis of at least three independent experiments with a single active $InsP_3R1$ in the bilayer was performed to generate the data for Table 1.

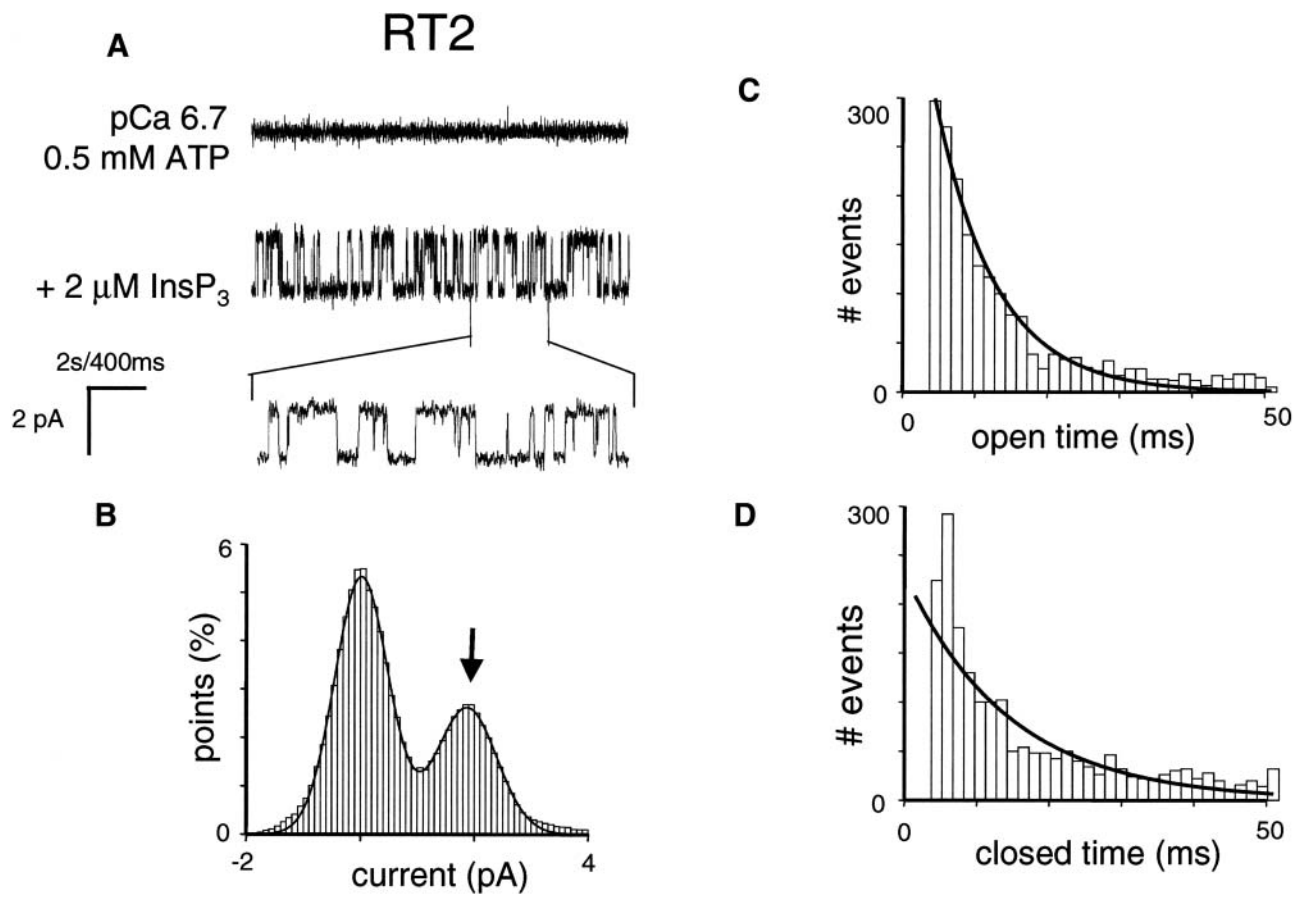

FIGURE 3 Single-channel properties of recombinant rat $InsP_3R2$ (*RT2*). (*B*) Single-channel records of recombinant $InsP_3R2$ in planar lipid bilayers. The experiments were performed at pCa 6.7 in the presence of 0.5 mM ATP (*top trace*). Addition of 2 μM $InsP_3$ to the *cis* (cytoplasmic) side activated $InsP_3R2$ (*middle trace*). Current trace at the expanded timescale is also shown (*bottom trace*). (*B–D*) Analysis of the single-channel records of $InsP_3R2$ was performed and analyzed as described for $InsP_3R1$ in the Fig. 2 legend. The Gaussian peak corresponding to an open state of $InsP_3R2$ (*arrow*) was centered at 1.89 pA, had $\sigma = 0.53$ pA, and area 35%. Open and closed time distributions (*C* and *D*; number of events = 5000) were fitted with a single exponential function (*curves*) that yielded mean open time $\tau_0 = 7.6$ ms and mean closed time $\tau_C = 10.8$ ms. The data from the same experiment were used for panels *A–D*. Similar analysis of at least three independent experiments with a single active $InsP_3R2$ in the bilayer was performed to generate the data for Table 1.

in the same experiment as described in Materials and Methods and the normalized data from different experiments with each $InsP_3R$ isoform were averaged together for presentation and analysis. Consistent with the previous findings (Lupu et al., 1998; Tang et al., 2003; Watras et al., 1991) we found that the open probability of $InsP_3R1$ was elevated with increase in $InsP_3$ concentration (Fig. 6, *open circles*). Fit to the RT1 data using Eq. 1 (Fig. 6, *curve*, $R^2 = 0.99$) yielded an apparent affinity $k_{InsP3} = 0.27 \pm 0.07$ μM $InsP_3$ (Table 2). When compared to $InsP_3R1$, $InsP_3R2$ were more sensitive to activation by $InsP_3$ (Fig. 6, *solid triangles*). Fit to the RT2 data using Eq. 1 (Fig. 6, *smooth curve*, $R^2 = 0.98$) yielded an apparent affinity $k_{InsP3} = 0.10 \pm 0.01$ μM $InsP_3$ (Table 2). In contrast, $InsP_3R3$ were least sensitive to activation by $InsP_3$ (Fig. 6, *solid circles*). Fit to the RT3 data using Eq. 1 (Fig. 6, *curve*, $R^2 = 0.98$) yielded an apparent affinity $k_{InsP3} = 0.40 \pm 0.05$ μM $InsP_3$ (Table 2).

Modulation of mammalian $InsP_3R$ isoforms by ATP

$InsP_3R1$ is allosterically activated by ATP (Bezprozvanny and Ehrlich, 1993; Ferris et al., 1990; Iino, 1991; Maes et al., 2000; Tu et al., 2002). Does ATP affect gating of other $InsP_3R$ isoforms? To investigate isoform-specific modulation of $InsP_3R$ by ATP, we measured ATP sensitivity of channel gating for the three mammalian $InsP_3R$ isoforms in the presence of 2 μM $InsP_3$ at pCa 6.7 and in the range of ATP concentrations from 0 to 2.5 mM for $InsP_3R1$ and from 0 to 5 mM for $InsP_3R2$ and $InsP_3R3$. In agreement with the previous findings (Bezprozvanny and Ehrlich, 1993; Ferris et al., 1990; Iino 1991; Maes et al., 2000; Tu et al., 2002) we found that activity of RT1 channels was potentiated by submillimolar ATP (Fig. 7 *A*). In contrast, the gating of RT2 channels was ATP independent (Fig. 7 *B*). Activity of RT3

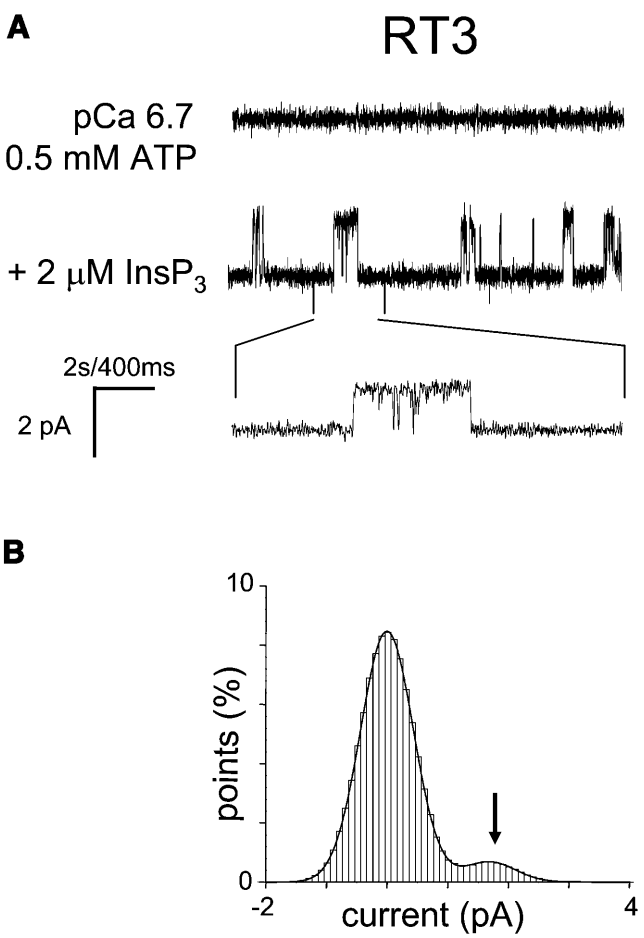

FIGURE 4 Single-channel properties of recombinant rat $InsP_3R3$ (*RT3*). (*A*) Single-channel records of recombinant $InsP_3R3$ in planar lipid bilayers. The experiments were performed at pCa 6.7 in the presence of 0.5 mM ATP (*top trace*). Addition of 2 μM $InsP_3$ to the *cis* (cytoplasmic) side activated $InsP_3R3$ (*middle trace*). Current trace at the expanded timescale is also shown (*bottom trace*). (*B*) Amplitude histogram of $InsP_3R3$ was generated as described for $InsP_3R1$ in the Fig. 2 *B* legend. The Gaussian peak corresponding to an open state of $InsP_3R3$ (*arrow*) was centered at 1.76 pA, had $\sigma = 0.43$ pA, and area 7%. The data from the same experiment were used for panels *A* and *B*. Similar analysis of at least three independent experiments with a single active $InsP_3R3$ in the bilayer was performed to generate the data for Table 1.

channels was elevated in the presence of ATP, but ATP concentrations in excess of 2 mM were required (Fig. 7 *C*). Most of the experiments resulted in multichannel bilayers. Thus, to analyze obtained results quantitatively, the *Po* values in each experiment were normalized to the maximal *Po* in the same experiment as described in Materials and Methods and the normalized data from different experiments with each $InsP_3R$ isoform were averaged together at each ATP concentration. Consistent with previous findings, we found that millimolar ATP increases RT1 activity approximately fivefold (Fig. 8, *open circles*). Fit to the RT1 data using Eq. 2 (see Materials and Methods) (Fig. 8, *curve*, $R^2 = 0.95$) indicated that an apparent affinity of $InsP_3R1$ for ATP

TABLE 1 Single-channel properties of mammalian $InsP_3R$ isoforms

$InsP_3R$	ATP (mM)	*Po* (%)	*i* (pA)	τ_o (mS)	τ_c (mS)	γ (pS)
RT1	0.5	33 ± 5	1.9 ± 0.1	7.0 ± 0.3	9.9 ± 1.3	80.0 ± 0.3
RT2	0.5	27 ± 6	1.9 ± 0.1	7.3 ± 0.4	10.6 ± 1.6	78.0 ± 0.5
RT3	0.5	4 ± 1	1.91 ± 0.04	ND	ND	74.0 ± 0.4
	5	33 ± 9	1.8 ± 0.2	7.4 ± 1.2	9.8 ± 1.1	ND

ND, not determined.

(k_{ATP}) is equal to 0.13 ± 0.04 mM and the effects of ATP on $InsP_3R1$ are not cooperative ($n_{Hill} = 1.3$) (Table 2). The parameter $(Pm + P0)/P0$ in Table 2 reflects a degree of ATP-dependent potentiation of $InsP_3R$ gating. Similar to RT1, RT3 activity was increased approximately sevenfold in the presence of ATP (Fig. 8, *solid circles*). Fit to the RT3 data using Eq. 2 (Fig. 8, *curve*, $R^2 = 0.98$) indicated that an apparent affinity of $InsP_3R3$ for ATP is equal to 2.0 ± 0.1 mM and the effects of ATP are highly cooperative ($n_{Hill} = 4.1$) (Table 2). In contrast with RT1 and RT3, gating of RT2 was ATP independent (Fig. 8, *solid triangles*).

Relatively low sensitivity of RT3 channels to ATP (Fig. 8, *solid circles*) indicated that 0.5 mM ATP used in standard recording conditions corresponds to suboptimal ATP concentration for $InsP_3R3$ activation. Thus, we repeated single-channel analysis of RT3-supported currents at pCa 6.7 in the presence of 2 μM $InsP_3$ and 5 mM ATP (Fig. 9 *A*). In these conditions, *Po* of $InsP_3R3$ was equal to 33 ± 9% ($n = 3$) (Fig. 9 *B*; Table 1), the size of the unitary current at 0 mV was equal to 1.8 ± 0.1 pA ($n = 3$) (Fig. 9 *B*; Table 1), the mean open dwell time was equal to 7 ± 1 ms ($n = 3$) (Fig. 9 *C*; Table 1), and the mean closed time was equal to 10 ± 1 ms ($n = 3$) (Fig. 9 *D*; Table 1). Thus, gating properties and open probability of RT3 channels in the presence of 5 mM ATP are similar to gating properties and open probability of RT1 and RT2 channels recorded in the presence of 0.5 mM ATP (Figs. 2, 3, and 9; Table 1).

DISCUSSION

Functional properties of mammalian $InsP_3R$ isoforms

All three mammalian $InsP_3R$ isoforms analyzed in our study expressed efficiently in Sf9 cells using baculoviral infection (Fig. 1) and formed $InsP_3$-gated channels in planar lipid bilayers (Figs. 2 *A*, 3 *A*, and 4 *A*). With 50 mM Ba^{2+} as a current carrier the size of the unitary current for all three mammalian $InsP_3R$ isoforms was equal to 1.9 pA at 0 mV transmembrane potential (Figs. 2 *B*, 3 *B*, and 4 *B*; Table 1). The single-channel conductance for three mammalian $InsP_3R$ isoforms was in the range 74–80 pS (Fig. 5; Table 1). In standard recording conditions (pCa 6.7, 2 μM $InsP_3$, and 0.5 mM ATP on the cytosolic side of the membrane) the single-channel open probability (*Po*) of the $InsP_3R1$ and

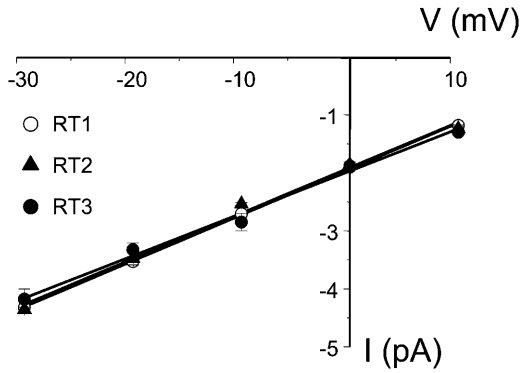

FIGURE 5 Current-voltage relationship of mammalian $InsP_3R$ isoforms. $InsP_3R$ currents were recorded in the planar lipid bilayers in the range of transmembrane potentials from −30 mV to +10 mV (*cis* versus *trans*). Single-channel current amplitude at each voltage was determined from a Gaussian fit as shown in Figs. 2 *B*, 3 *B*, and 4 *B*. The data for RT1 (○), RT2 (▲), and RT3 (●) are shown as means ± SE ($n \geq 3$). The slope of the linear fit to the data (*lines*; $r = 0.99$) yielded a single-channel conductance of 80 pS for RT1, 78 pS for RT2, and 74 pS for RT3.

$InsP_3R2$ channels was ~30% (Figs. 2 *B* and 3 *B*; Table 1), whereas *Po* of $InsP_3R3$ was <5% (Fig. 4 *B*; Table 1). In the same recording conditions the mean open dwell time of $InsP_3R1$ and $InsP_3R2$ was in the range 7–8 ms (Figs. 2 *C* and 3 *C*; Table 1) and the mean closed time was ~10 ms (Figs. 2 *D* and 3 *D*; Table 1). When ATP dependence of $InsP_3R$ isoforms was compared (Figs. 7 and 8; Table 2), we found that 0.5 mM ATP maximally activated $InsP_3R1$, but was not sufficient for maximal activation of $InsP_3R3$. We also found that gating of $InsP_3R2$ was ATP independent. In the presence of pCa 6.7, 2 μM $InsP_3$ and 5 mM ATP on the cytosolic side of the membrane *Po* of $InsP_3R3$ was elevated to 30% (Fig. 9 *B*; Table 1), the mean open time was equal to 8 ms (Fig. 9 *C*; Table 1) and the mean closed time was equal to 10 ms (Fig. 9

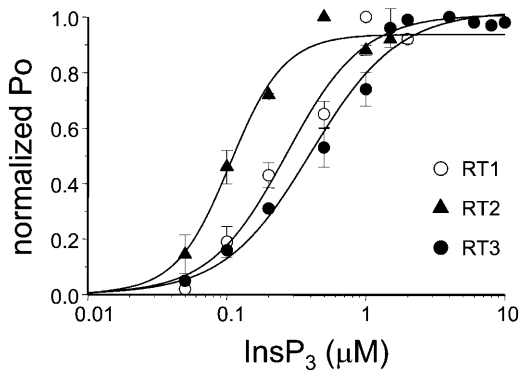

FIGURE 6 $InsP_3$ sensitivity of mammalian $InsP_3R$ isoforms. The single-channel open probability (*Po*) for each $InsP_3R$ isoform was measured as a function of $InsP_3$ concentrations on the *cis* (cytoplasmic) side of the membrane at pCa 6.7 in the presence of 0.5 mM ATP. The normalized and averaged data (see Materials and Methods) are shown as means ± SE ($n \geq 3$) for RT1 (○), RT2 (▲), and RT3 (●). The data were fitted using Eq. 1 (see Materials and Methods). The parameters of the best fit (*curves*) are in Table 2.

TABLE 2 $InsP_3$ and ATP sensitivity of mammalian $InsP_3R$ isoforms

	$InsP_3$ dependence		ATP dependence		
$InsP_3R$	k_{InsP3} (μM)	n_{Hill}	k_{ATP} (mM)	n_{Hill}	$(Pm + P0)/P0$
RT1	0.27 ± 0.07	1.6	0.13 ± 0.04	1.3	5.26
RT2	0.10 ± 0.01	2.2	N/A	N/A	N/A
RT3	0.40 ± 0.05	1.4	2.0 ± 0.1	4.1	7.14

N/A, not applicable.

Parameters k_{InsP3} and n_{Hill} ($InsP_3$ dependence) were determined from the best fit to the data shown on Fig. 6 using Eq. 1, parameters k_{ATP}, n_{Hill}, *P0*, and *Pm* (ATP dependence) were determined from the best fit to the data shown on Fig. 8 using Eq. 2.

D; Table 1). Thus, all three mammalian $InsP_3R$ isoforms display similar maximal open probability in optimal recording conditions (~30%) and share common gating and conductance properties (Table 1). The similarity in conductance and gating properties is consistent with the high degree of sequence conservation in channel-forming carboxy-terminal domain of $InsP_3R$ (Furuichi et al., 1994) and with the previous single-channel studies (Hagar et al., 1998; Mak et al., 2000; Ramos-Franco et al., 2000, 1998). In a recent study we described functional properties of recombinant *Drosophila melanogaster* $InsP_3R$ ($DmInsP_3R$) expressed in Sf9 cells by baculoviral infection and reconstituted into planar lipid bilayers (Srikanth et al., 2004). We found that $DmInsP_3R$ displayed conductance and gating properties remarkably similar to mammalian $InsP_3R$ isoforms (Srikanth et al., 2004), indicating that these major functional properties of $InsP_3R$ are conserved in evolution.

The three mammalian $InsP_3R$ isoforms differ in sensitivity to activation by $InsP_3$ (Fig. 6; Table 2). The $InsP_3R2$ isoform is most sensitive to activation by $InsP_3$ ($k_{InsP3} = 0.10$ μM), followed by $InsP_3R1$ ($k_{InsP3} = 0.27$ μM $InsP_3$), and then by $InsP_3R3$ ($k_{InsP3} = 0.40$ μM $InsP_3$) (Fig. 6; Table 2). The differences in apparent affinities of mammalian $InsP_3R$ isoforms to activation by $InsP_3$ observed in our experiments are consistent with the functional analysis of $InsP_3R$ isoforms in DT40 cells (Miyakawa et al., 1999), and with the [^{3}H]$InsP_3$ binding (Maranto, 1994; Ramos-Franco et al., 2000; Sudhof et al., 1991) (but see Nerou et al., 2001) and single-channel (Hagar and Ehrlich, 2000; Ramos-Franco et al., 2000) studies.

The three mammalian $InsP_3R$ isoforms also differ in sensitivity to allosteric modulation by ATP (Figs. 7 and 8; Table 2). Search for potential ATP-binding sites with the query G*X*G*XX*G (Wierenga and Hol, 1983) reveals a presence of two potential ATP-binding sites in the $InsP_3R1$ sequence ^{1773}GGGGGGPG^{1780} (ATPA) and ^{2015}GGLGLLG^{2021} (ATPB); two potential ATP-binding sites in the $InsP_3R2$ sequence ^{1727}GGGFTG^{1732} (ATPA) and ^{1968}GGLGLLG^{1974} (ATPB); and a single potential ATP-binding site in the $InsP_3R3$ sequence ^{1919}GGLGLLG^{1925} (ATPB). Previous biochemical experiments indicated that the ATPA site in the $InsP_3R1$ sequence binds ATP with high affinity (Maes et al., 1999) and

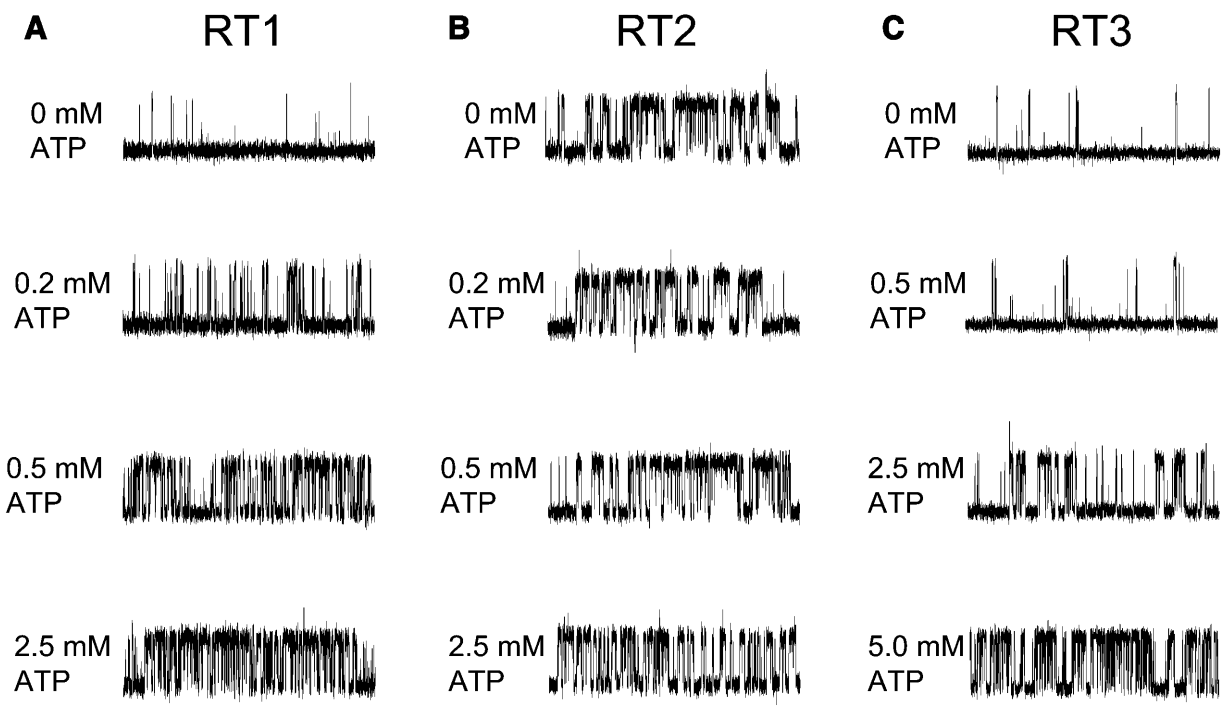

FIGURE 7 ATP sensitivity of mammalian $InsP_3R$ isoforms. Representative current records of RT1 (*A*), RT2 (*B*), and RT3 (*C*) channels in the bilayers in the presence of 2 μM $InsP_3$ and pCa 6.7 at concentrations of Na_2ATP as indicated on the *cis* (cytoplasmic) side of the membrane. The recordings from the same experiment are shown on each panel. Similar results were obtained in at least three experiments with each $InsP_3R$ isoform.

ATPB sites in $InsP_3R1$ and $InsP_3R3$ bind ATP with low affinity (Maes et al., 2001, 1999). ATP-binding properties of ATPA and ATPB sites in $InsP_3R2$ have not been examined in biochemical experiments. We found that both $InsP_3R1$ and $InsP_3R3$ are activated approximately fivefold by ATP, whereas $InsP_3R2$ does not depend on ATP for maximal activation (Figs. 7 and 8). In agreement with the previous functional studies of $InsP_3R1$ (Bezprozvanny and Ehrlich, 1993; Ferris et al., 1990; Iino, 1991; Maes et al., 2000; Tu et al., 2002), we found that the $InsP_3R1$ apparent affinity for ATP is high ($k_{ATP} = 0.13$ mM) and effects of ATP are not cooperative ($n_{Hill} = 1.3$) (Fig. 8; Table 2). Also in agreement with the previous functional studies of $InsP_3R3$ (Hagar and Ehrlich, 2000; Maes et al., 2000; Mak et al., 2001a; Missiaen et al., 1998), we found that the $InsP_3R3$ apparent affinity for ATP is low ($k_{ATP} = 2$ mM) (Fig. 8; Table 2). We also discovered that effects of ATP on $InsP_3R3$ are highly cooperative ($n_{Hill} = 4.1$) (Fig. 8; Table 2). High sensitivity of $InsP_3R1$ to modulation by ATP most likely results from the unique high-affinity ATPA site (Bezprozvanny and Ehrlich, 1993; Ferris et al., 1990; Iino, 1991; Maes et al., 2000; Tu et al., 2002). Indeed, $InsP_3R1$ sensitivity to modulation by ATP was greatly reduced in the $InsP_3R1$-*opt* mutant that lacks ATPA site (Tu et al., 2002). Low sensitivity of $InsP_3R3$ to modulation by ATP is consistent with low affinity of the ATPB binding site, which is likely to account for modulation of $InsP_3R3$ by ATP. We would like to suggest that due to low affinity and high cooperativity, $InsP_3R3$ regulation by ATP may be important in a physiological range of intracellular ATP concentrations (~2 mM). This idea is consistent with predominant $InsP_3R3$ expression in pancreatic β-cells (Taylor et al., 1999). We would like to propose that ATP modulation of $InsP_3R3$ in pancreatic β-cells may play a role in control of glucose-dependent insulin secretion. ATP modulation of $InsP_3R1$ is more likely to play a role in pathological

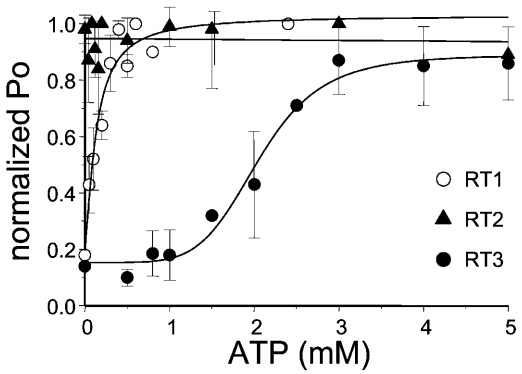

FIGURE 8 ATP modulation of mammalian $InsP_3R$ isoforms. The single-channel open probability (*Po*) for each $InsP_3R$ isoform was measured as a function of Na_2ATP concentrations on the *cis* (cytoplasmic) side of the membrane at pCa 6.7 in the presence of 2 μM $InsP_3$. The normalized and averaged data (see Materials and Methods) are shown as means ± SE ($n \geq 3$) for RT1 (○), RT2 (▲), and RT3 (●). The data for RT1 and RT3 were fit by Eq. 2 (see Materials and Methods). The parameters of the best fit (*curves*) are in Table 2. The data for RT2 were fit by a linear regression (*line*).

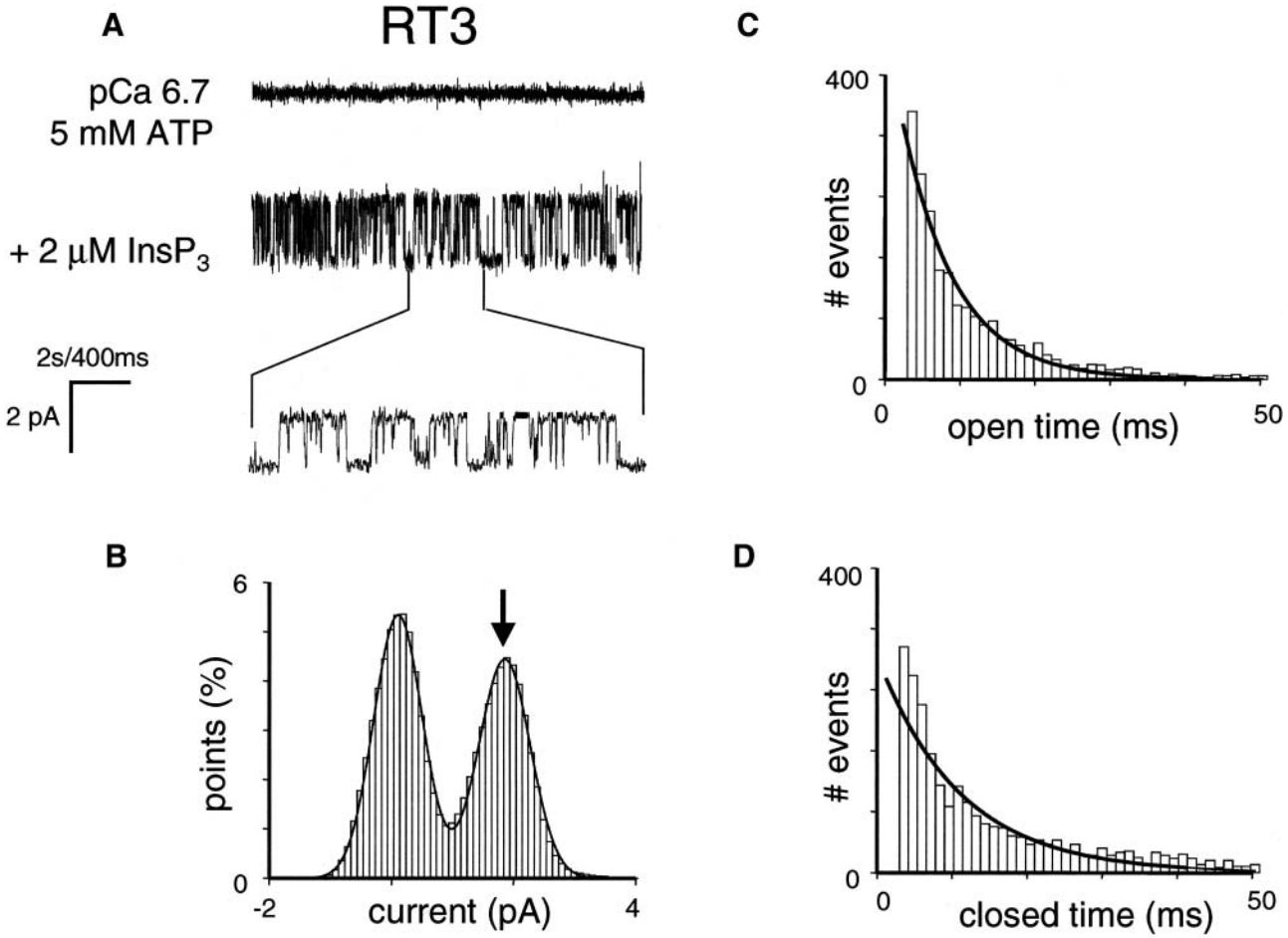

FIGURE 9 Single-channel properties of recombinant rat $InsP_3R3$ (RT3) at 5 mM ATP. Single-channel records of recombinant $InsP_3R3$ in planar lipid bilayers. The experiments were performed at pCa 6.7 in the presence of 5 mM ATP (*top trace*). Addition of 2 μM $InsP_3$ to the *cis* (cytoplasmic) side activated $InsP_3R3$ (*middle trace*). Current trace at the expanded timescale is also shown (*bottom trace*). (*B–D*) Analysis of the single-channel records of $InsP_3R3$ was performed and analyzed as described for $InsP_3R1$ in the Fig. 2 legend. The Gaussian peak corresponding to an open state of $InsP_3R3$ (*arrow*) was centered at 1.84 pA, had $\sigma = 0.34$ pA, and area 47%. Open and closed time distributions (*C* and *D*; number of events = 5000) were fitted with a single exponential function (*curves*) that yielded mean open time $\tau_0 = 7.8$ ms and mean closed time $\tau_C = 10.2$ ms. The data from the same experiment were used for panels *A–D*. Similar analysis of at least three independent experiments with a single active $InsP_3R3$ in bilayer was performed to generate the data for Table 1.

conditions such as ischemia, when ATP concentrations can fall below 0.1 mM (Abe et al., 1987). Despite the presence of both ATPA and ATPB putative ATP-binding sites in the $InsP_3R2$ sequence, $InsP_3R2$ gating is ATP independent (Figs. 7 and 8). The ATP sensitivity of $InsP_3R2$ has not been previously examined in electrophysiological experiments. However, in agreement with our findings, $InsP_3R2$ was not modulated by ATP in Ca^{2+} flux experiments with DT40 cells (Miyakawa et al., 1999).

We are grateful to Gregory Mignery and Thomas C. Südhof for the kind gift of the rat $InsP_3R1$ and $InsP_3R2$ clones, to Dr. Graeme Bell for the kind gift of the rat $InsP_3R3$ clone. We thank Phyllis Foley for the administrative assistance.

This work was supported by the Welch Foundation and National Institutes of Health (R01 NS38082 to I.B.) and the Fund for Scientific Research, Flanders, Belgium (G.0210.03 to H.D.S.).

REFERENCES

Abe, K., K. Kogure, H. Yamamoto, M. Imazawa, and K. Miyamoto. 1987. Mechanism of arachidonic acid liberation during ischemia in gerbil cerebral cortex. *J. Neurochem.* 48:503–509.

Berridge, M. J. 1993. Inositol trisphosphate and calcium signalling. *Nature.* 361:315–325.

Bezprozvanny, I., and B. E. Ehrlich. 1993. ATP modulates the function of inositol 1,4,5-trisphosphate-gated channels at two sites. *Neuron.* 10:1175–1184.

Bezprozvanny, I., and B. E. Ehrlich. 1994. Inositol (1,4,5)-trisphosphate ($InsP_3$)-gated Ca channels from cerebellum: conduction properties for divalent cations and regulation by intraluminal calcium. *J. Gen. Physiol.* 104:821–856.

Bezprozvanny, I., and B. E. Ehrlich. 1995. The inositol 1,4,5-trisphosphate ($InsP_3$) receptor. *J. Membr. Biol.* 145:205–216.

Colquhoun, D., and A. G. Hawkes. 1983. The principles of stochastic interpretation of ion-channel mechanisms. *In* Single-Channel Recording. B. Sakmann and E. Neher, editors. Plenum Press, New York. 135–174.

Dempster, J. 2001. The Laboratory Computer: A Practical Guide for Neuroscientists and Physiologists. Academic Press, New York.

Ferris, C. D., R. L. Huganir, and S. H. Snyder. 1990. Calcium flux mediated by purified inositol 1,4,5-trisphosphate receptor in reconstituted lipid vesicles is allosterically regulated by adenine nucleotides. *Proc. Natl. Acad. Sci. USA*. 87:2147–2151.

Furuichi, T., K. Kohda, A. Miyawaki, and K. Mikoshiba. 1994. Intracellular channels. *Curr. Opin. Neurobiol*. 4:294–303.

Hagar, R. E., A. D. Burgstahler, M. H. Nathanson, and B. E. Ehrlich. 1998. Type III InsP3 receptor channel stays open in the presence of increased calcium. *Nature*. 396:81–84.

Hagar, R. E., and B. E. Ehrlich. 2000. Regulation of the type III InsP(3) receptor by InsP(3) and ATP. *Biophys. J*. 79:271–278.

Horn, R. 1991. Estimating the number of channels in patch recordings. *Biophys. J*. 60:433–439.

Iino, M. 1991. Effects of adenine nucleotides on inositol 1,4,5-trisphosphate-induced calcium release in vascular smooth muscle cells. *J. Gen. Physiol*. 98:681–698.

Kaznacheyeva, E., V. D. Lupu, and I. Bezprozvanny. 1998. Single-channel properties of inositol (1,4,5)-trisphosphate receptor heterologously expressed in HEK-293 cells. *J. Gen. Physiol*. 111:847–856.

Lupu, V. D., E. Kaznacheyeva, U. M. Krishna, J. R. Falck, and I. Bezprozvanny. 1998. Functional coupling of phosphatidylinositol 4,5-bisphosphate to inositol 1,4,5-trisphosphate receptor. *J. Biol. Chem*. 273:14067–14070.

Maes, K., L. Missiaen, P. De Smet, S. Vanlingen, G. Callewaert, J. B. Parys, and H. De Smedt. 2000. Differential modulation of inositol 1,4,5-trisphosphate receptor type 1 and type 3 by ATP. *Cell Calcium*. 27:257–267.

Maes, K., L. Missiaen, J. B. Parys, P. De Smet, I. Sienaert, E. Waelkens, G. Callewaert, and H. De Smedt. 2001. Mapping of the ATP-binding sites on inositol 1,4,5-trisphosphate receptor type 1 and type 3 homotetramers by controlled proteolysis and photoaffinity labeling. *J. Biol. Chem*. 276:3492–3497.

Maes, K., L. Missiaen, J. B. Parys, I. Sienaert, G. Bultynck, M. Zizi, P. De Smet, R. Casteels, and H. De Smedt. 1999. Adenine-nucleotide binding sites on the inositol 1,4,5-trisphosphate receptor bind caffeine, but not adenophostin A or cyclic ADP-ribose. *Cell Calcium*. 25:143–152.

Mak, D. O., S. McBride, and J. K. Foskett. 2001a. ATP regulation of recombinant type 3 inositol 1,4,5-trisphosphate receptor gating. *J. Gen. Physiol*. 117:447–456.

Mak, D. O., S. McBride, and J. K. Foskett. 2001b. Regulation by Ca2+ and inositol 1,4,5-trisphosphate (InsP3) of single recombinant type 3 InsP3 receptor channels. Ca2+ activation uniquely distinguishes types 1 and 3 InsP3 receptors. *J. Gen. Physiol*. 117:435–446.

Mak, D. O., S. McBride, V. Raghuram, Y. Yue, S. K. Joseph, and J. K. Foskett. 2000. Single-channel properties in endoplasmic reticulum membrane of recombinant type 3 inositol trisphosphate receptor. *J. Gen. Physiol*. 115:241–256.

Maranto, A. R. 1994. Primary structure, ligand binding, and localization of the human type 3 inositol 1,4,5-trisphosphate receptor expressed in intestinal epithelium. *J. Biol. Chem*. 269:1222–1230.

Mignery, G. A., and T. C. Sudhof. 1990. The ligand binding site and transduction mechanism in the inositol-1,4,5-triphosphate receptor. *EMBO J*. 9:3893–3898.

Miller, C. 1986. Ion Channel Reconstitution. C. Miller, editor. Plenum Press, New York.

Missiaen, L., J. B. Parys, I. Sienaert, K. Maes, K. Kunzelmann, M. Takahashi, K. Tanzawa, and H. De Smedt. 1998. Functional properties of the type-3 InsP3 receptor in 16HBE14o- bronchial mucosal cells. *J. Biol. Chem*. 273:8983–8986.

Miyakawa, T., A. Maeda, T. Yamazawa, K. Hirose, T. Kurosaki, and M. Iino. 1999. Encoding of Ca2+ signals by differential expression of IP3 receptor subtypes. *EMBO J*. 18:1303–1308.

Miyawaki, A., T. Furuichi, Y. Ryou, S. Yoshikawa, T. Nakagawa, T. Saitoh, and K. Mikoshiba. 1991. Structure-function relationships of the mouse inositol 1,4,5- trisphosphate receptor. *Proc. Natl. Acad. Sci. USA*. 88:4911–4915.

Nerou, E. P., A. M. Riley, B. V. Potter, and C. W. Taylor. 2001. Selective recognition of inositol phosphates by subtypes of the inositol trisphosphate receptor. *Biochem. J*. 355:59–69.

Nosyreva, E., T. Miyakawa, Z. Wang, L. Glouchankova, A. Mizushima, M. Iino, and I. Bezprozvanny. 2002. The high affinity calcium-calmodulin-binding site does not play a role in modulation of type 1 inositol (1,4,5)-trisphosphate receptor function by calcium and calmodulin. *Biochem. J*. 365:659–667.

Ramos-Franco, J., D. Bare, S. Caenepeel, A. Nani, M. Fill, and G. Mignery. 2000. Single-channel function of recombinant type 2 inositol 1,4, 5-trisphosphate receptor. *Biophys. J*. 79:1388–1399.

Ramos-Franco, J., M. Fill, and G. A. Mignery. 1998. Isoform-specific function of single inositol 1,4,5-trisphosphate receptor channels. *Biophys. J*. 75:834–839.

Sakmann, B., and E. Neher. 1983. Single-Channel Recording. B. Sakmann and E. Neher, editors. Plenum Press, New York.

Srikanth, S., Z. Wang, H. Tu, S. Nair, M. K. Mathew, G. Hasan, and I. Bezprozvanny. 2004. Functional properties of the *Drosophila melanogaster* inositol 1,4,5-trisphosphate receptor mutants. *Biophys. J*. 86: 3634–3646.

Sudhof, T. C., C. L. Newton, B. T. Archer, Y. A. Ushkaryov, and G. A. Mignery. 1991. Structure of a novel $InsP_3$ receptor. *EMBO J*. 10:3199–3206.

Tang, T. S., H. Tu, Z. Wang, and I. Bezprozvanny. 2003. Modulation of type 1 inositol (1,4,5)-trisphosphate receptor function by protein kinase A and protein phosphatase 1alpha. *J. Neurosci*. 23:403–415.

Taylor, C. W., A. A. Genazzani, and S. A. Morris. 1999. Expression of inositol trisphosphate receptors. *Cell Calcium*. 26:237–251.

Thrower, E. C., R. E. Hagar, and B. E. Ehrlich. 2001. Regulation of Ins(1,4,5)P3 receptor isoforms by endogenous modulators. *Trends Pharmacol. Sci*. 22:580–586.

Tu, H., T. Miyakawa, Z. Wang, L. Glouchankova, M. Iino, and I. Bezprozvanny. 2002. Functional characterization of the type 1 inositol 1,4,5-trisphosphate receptor coupling domain SII(+/−) splice variants and the *opisthotonos* mutant form. *Biophys. J*. 82:1995–2004.

Tu, H., E. Nosyreva, T. Miyakawa, Z. Wang, A. Mizushima, M. Iino, and I. Bezprozvanny. 2003. Functional and biochemical analysis of the type 1 inositol (1,4,5)-trisphosphate receptor calcium sensor. *Biophys. J*. 85:290–299.

Watras, J., I. Bezprozvanny, and B. E. Ehrlich. 1991. Inositol 1,4,5-trisphosphate-gated channels in cerebellum: presence of multiple conductance states. *J. Neurosci*. 11:3239–3245.

Wierenga, R. K., and W. G. Hol. 1983. Predicted nucleotide-binding properties of p21 protein and its cancer-associated variant. *Nature*. 302:842–844.